Supplemental data

Supplemental Figures 1-9

Supplemental Videos 1-4

Supplemental Tables 1-4

Supplemental Methods

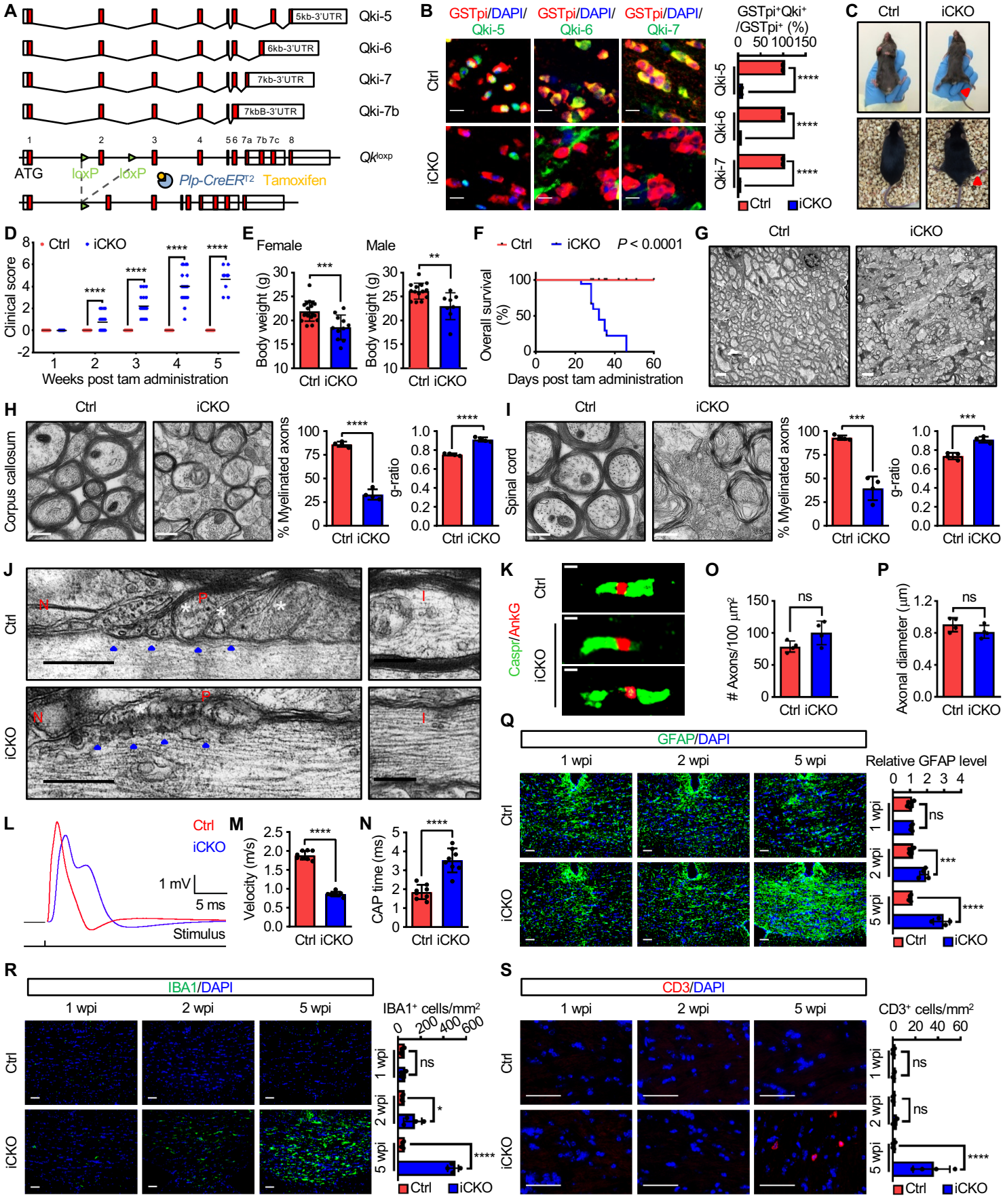

Supplemental Figure 1. Qki is essential for maintaining myelin integrity. (**A**) Schema depicting the splicing isoforms of *Qk* gene and the generation of oligodendrocyte-specific *Qk*-iCKO mice. 3'UTR, 3' untranslated region. (**B**) Representative images and quantification of immunofluorescent staining of GSTpi–Qki-5, GSTpi–Qki-6, and GSTpi–Qki-7 in the corpus callosum tissues of *Qk*-iCKO mice and controls 5 wpi ($n = 4$ mice/group). Scale bars, 10 µm. (**C**) Representative images showing the severe hind limb weakness and paresis of *Qk*-iCKO mice 4 wpi. (**D**) The clinical scores of *Qk*-iCKO mice ($n = 18$) and controls

(n = 34) are shown. Tam, tamoxifen. (**E**) Body weights of *Qk*-iCKO mice and controls 4 wpi (n = 18 female mice and n = 14 male mice in the control group. n = 11 female mice and n = 8 male mice in the *Qk*-iCKO group). (**F**) The Kaplan-Meier overall survival curves (log-rank test) of *Qk*-iCKO mice (n = 18) and controls (n = 34) are shown. (**G-I**) Representative electron micrographs of cross sections of the optic nerves (**G**), corpus callosum tissues (**H**), and spinal cords (**I**) of *Qk*-iCKO mice and controls 5 wpi (n = 4 mice/group). Scale bars, 2 μm (**G**); 500 nm (**H** and **I**). (**J**) Representative electron micrographs of longitudinal sections of the optic nerves from *Qk*-iCKO mice and controls 5 wpi. The node (N), paranode (P, *), internode (I), and axoglial junction (arrowhead) are indicated. Scale bars, 500 nm. (**K**) Representative images of immunofluorescent staining of Caspr and AnkG in the optic nerves of *Qk*-iCKO mice and controls 5 wpi. Scale bars, 1 μm. (**L-N**) Representative CAP traces (**L**) and quantification of conduction velocities (**M**) and CAP time (**N**) recorded from Qk-iCKO mice and controls 5 wpi. n = 4 mice/group, n = 8 optic nerves/group. (**O** and **P**) Quantification of axon density (**O**) and axonal diameter (**P**) in the experimental mice in **G** (n = 4 mice/group). (**Q-S**) Representative images and quantification of immunofluorescent staining of GFAP (**Q**), IBA1 (**R**), and CD3 (**S**) in the corpus callosum tissues of *Qk*-iCKO mice and controls 1, 2, and 5 wpi (n = 4 mice/group). Scale bars, 50 μm. Data are mean ± s.d.; student's t test (**B**, **E**, **H**, **I**, and **M-P**); two-way ANOVA with Holm-Sidak's multiple comparisons test (**D** and **Q-S**). *P < 0.05; **P < 0.01; ***P < 0.001; ****P < 0.0001; ns, not significant.

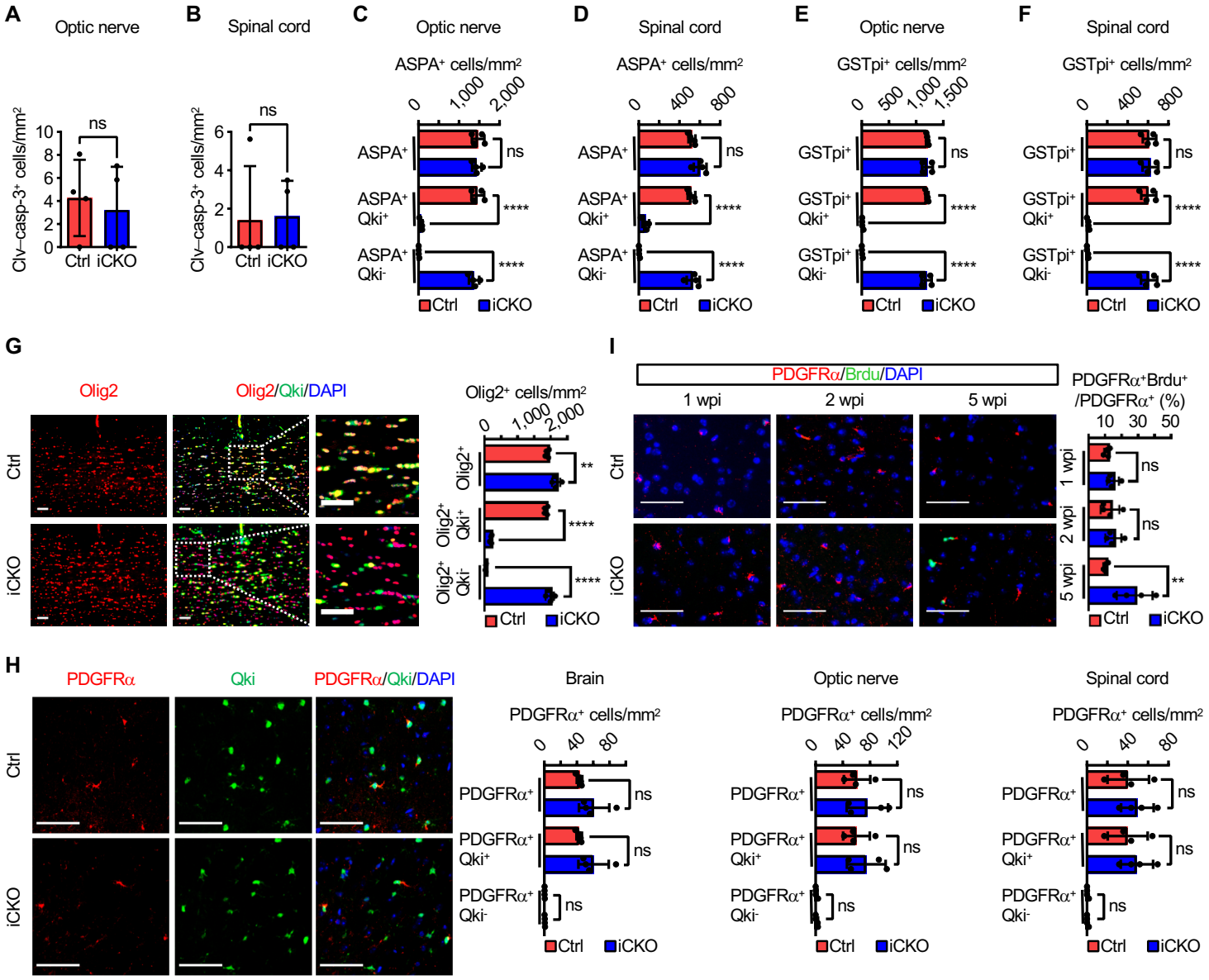

Supplemental Figure 2. Qki regulates myelin homeostasis independently of oligodendrocyte death. (**A** and **B**) Quantification of dead cells by immunofluorescent staining of Clv–casp-3 in the optic nerves and spinal cords of *Qk*-iCKO mice and controls 5 weeks after tamoxifen injection ($n = 4$ mice/group). (**C-F**) Quantification of immunofluorescent staining of ASPA-Qki and GSTpi-Qki in the optic nerves and spinal cords of *Qk*-iCKO mice and controls 5 weeks after tamoxifen injection ($n = 4$ mice/group). (**G**) Representative images and quantification of immunofluorescent staining of Olig2 and Qki in the corpus callosum tissues of *Qk*-iCKO mice and controls 5 weeks after tamoxifen injection ($n = 4$ mice/group). Scale bars, 50 μm. (**H**) Representative images and quantification of immunofluorescent staining of PDGFRα and Qki in the brains, optic nerves, and spinal cords of *Qk*-iCKO mice and controls 5 weeks after tamoxifen injection ($n = 4$ mice/group). Scale bars, 50 μm. (**I**) Representative images and quantification of immunofluorescent staining of PDGFRα and Brdu in the brains of *Qk*-iCKO mice and controls 1, 2, and 5 wpi ($n = 4$ mice/group). Scale bars, 50 μm. Data are mean ± s.d.; student's *t* test (**A** and **B**); one-way ANOVA followed by Bonferroni's post hoc test (**C-I**). $^{**}P < 0.01$; $^{****}P < 0.0001$; ns, not significant.

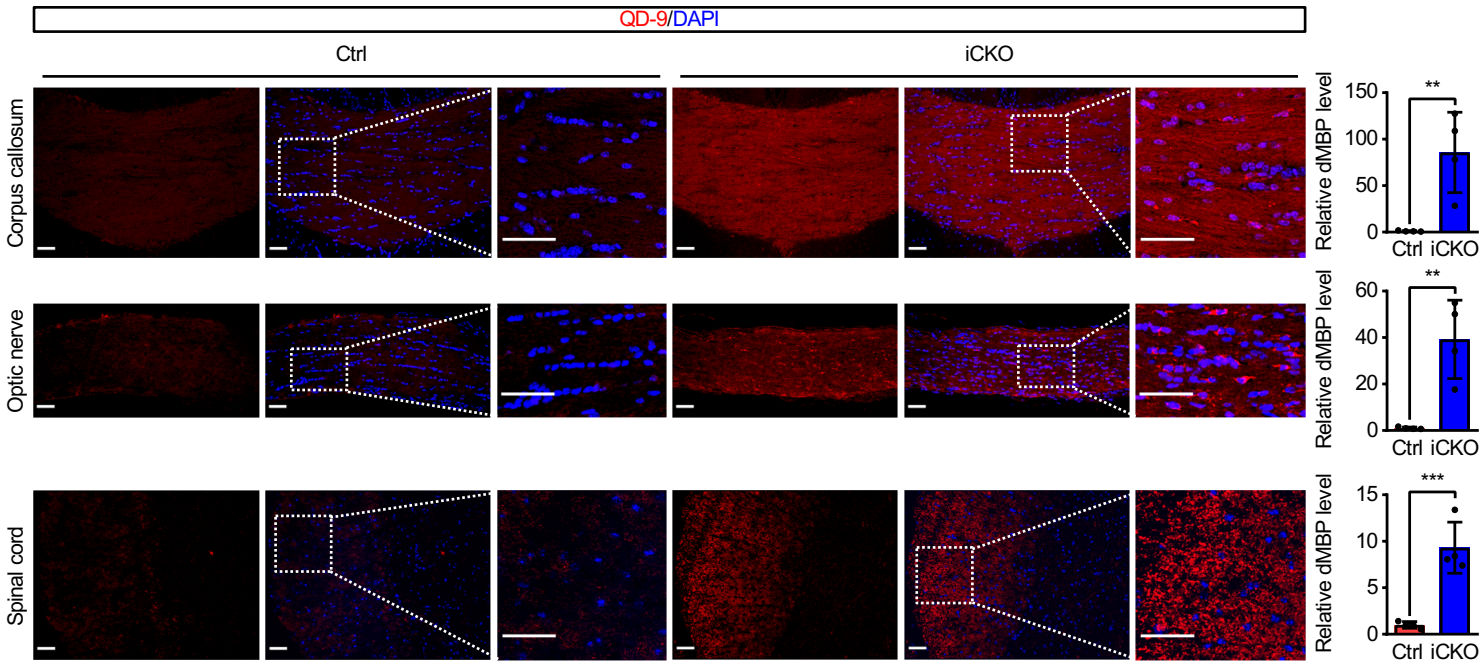

Supplemental Figure 3. Loss of Qki in mature oligodendrocytes leads to accumulation of degenerating myelin. Representative images and quantification of immunofluorescent staining of the QD-9 antibody in the corpus callosum tissues, optic nerves, and spinal cords of *Qk*-iCKO mice and controls 5 weeks post tamoxifen injection ($n = 4$ mice/group). Scale bars, 50 μm. Data are mean ± s.d.; student's t test. $^{**}P < 0.01$; $^{***}P < 0.001$.

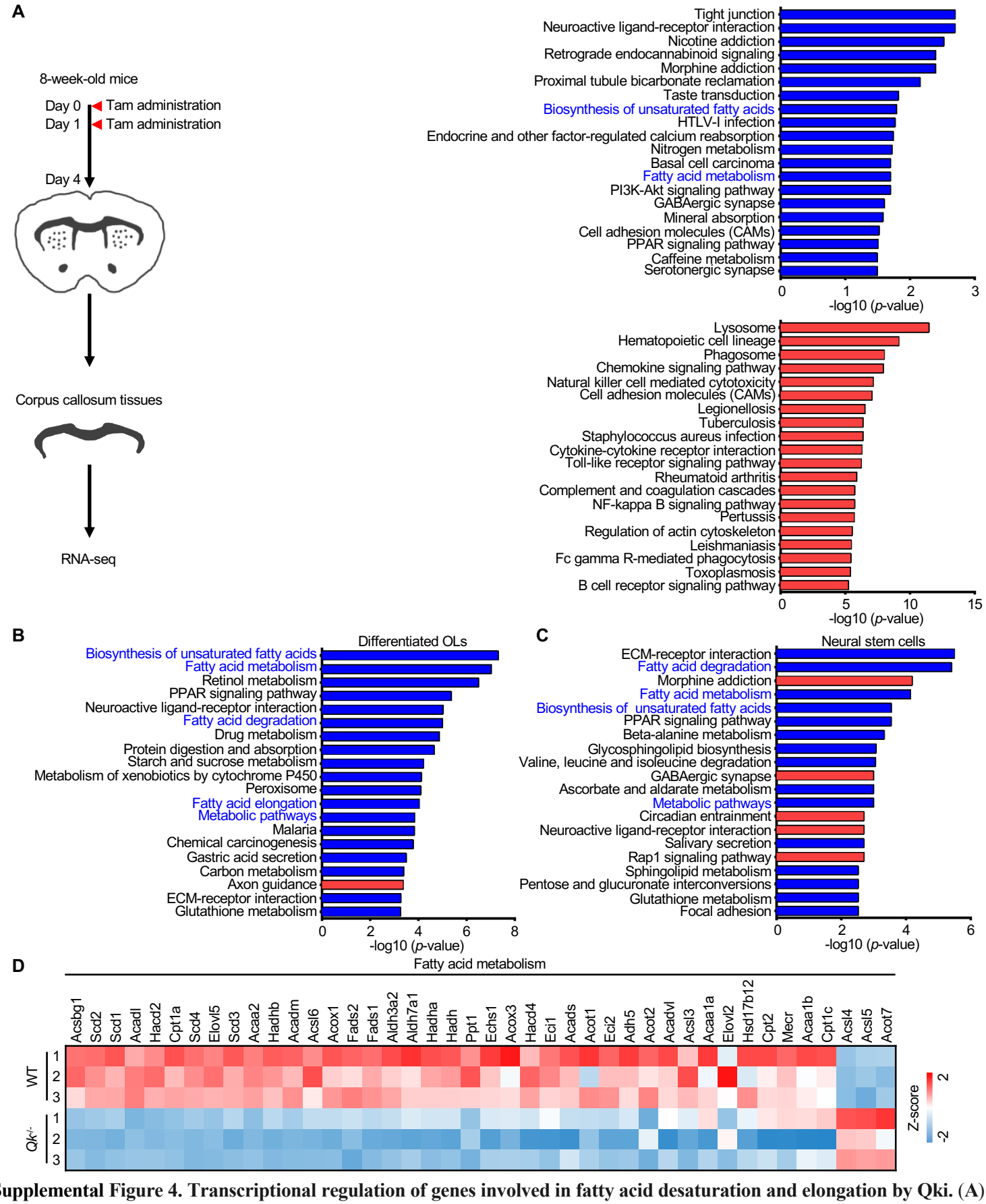

Supplemental Figure 4. Transcriptional regulation of genes involved in fatty acid desaturation and elongation by Qki. (**A**) Schema depicting the workflow for sample collection and RNA sequencing in the corpus callosum tissues of *Qk*-iCKO mice and controls (left). $n = 4$ mice/group. The top 20 enriched pathways are shown as bar graphs (right). (**B**) Bar graph showing the top 20 enriched pathways in WT and Qki-depleted differentiated oligodendrocytes ($n = 3$ cell lines/group). (**C**) Bar graph showing the top 20 enriched pathways in WT and Qki-depleted NSCs ($n = 4$ cell lines/group). Blue and red represent pathways whose activities were decreased or increased, respectively. (**D**) Heat map representing the differentially expressed genes involved in fatty acid metabolism in differentiated oligodendrocytes.

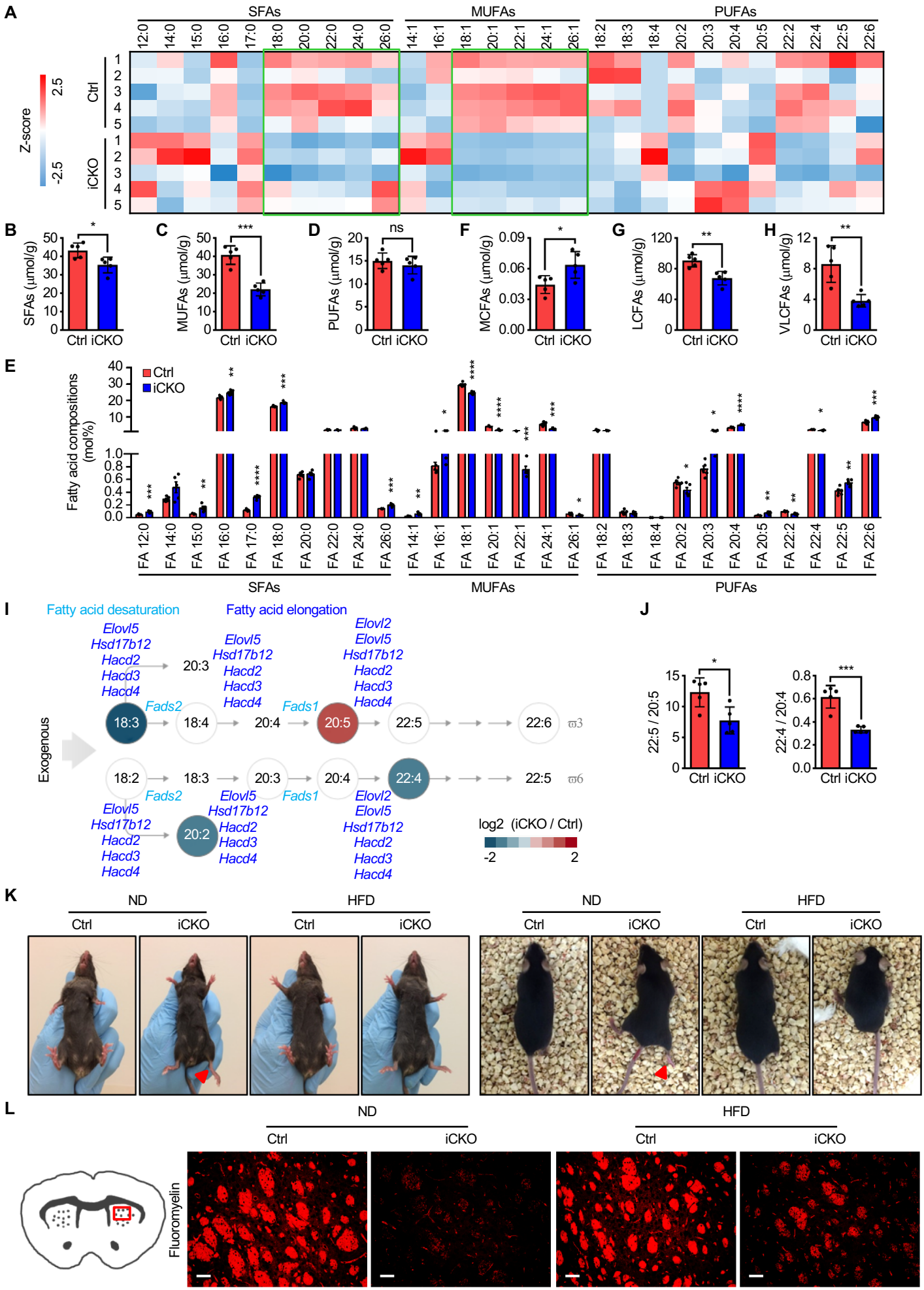
A
SFAs
MUFAs
PUFAs
12:0 14:0 15:0 16:0 17:0 18:0 20:0 22:0 24:0 26:0
14:1 16:1 18:1 20:1 22:1 24:1 26:1
18:2 18:3 18:4 20:2 20:3 20:4 20:5 22:2 22:4 22:5 22:6
Z-score
2.5
-2.5
Ctrl
iCKO
B SFAs (μmol/g)
C MUFAs (μmol/g)
D PUFAs (μmol/g)
ns
F MCFAs (μmol/g)
G LCFAs (μmol/g)
H VLCFAs (μmol/g)
Ctrl iCKO
E
Fatty acid compositions (mol%)
FA 12:0 FA 14:0 FA 15:0 FA 16:0 FA 17:0 FA 18:0 FA 20:0 FA 22:0 FA 24:0 FA 26:0
FA 14:1 FA 16:1 FA 18:1 FA 20:1 FA 22:1 FA 24:1 FA 26:1
FA 18:2 FA 18:3 FA 18:4 FA 20:2 FA 20:3 FA 20:4 FA 20:5 FA 22:2 FA 22:4 FA 22:5 FA 22:6
I
Fatty acid desaturation
Fatty acid elongation
Elovl5 Hsd17b12 Hacd2 Hacd3 Hacd4
Elovl2 Elovl5 Hsd17b12 Hacd2 Hacd3 Hacd4
Exogenous
18:3 18:4 20:4 20:5 22:5 22:6 ω3
18:2 18:3 20:3 20:4 22:4 22:5 ω6
20:2
Fads1
Fads2
log2 (iCKO / Ctrl)
-2 2
J
22:5 / 20:5
22:4 / 20:4
K
ND HFD
Ctrl iCKO
L
Fluoromyelin

Supplemental Figure 5. Disturbed fatty acid desaturation and elongation by depletion of Qki in mature oligodendrocytes. (**A**) Heat map plotting the differences in the concentrations of each fatty acid species as measured by mass spectrometry in the spinal cords of *Qk*-iCKO mice and controls 5 weeks after tamoxifen injection (n = 5 mice/group). The green boxes highlight the saturated and monounsaturated LCFAs and VLCFAs. (**B-D**) Quantification of the concentrations of SFAs (**B**), MUFAs (**C**), and PUFAs (**D**) in the samples in **A** (n = 5 mice/group). (**E**) Quantification of the compositions of fatty acids in the samples in **A** (n = 5 mice/group). (**F-H**) Quantification of the concentrations of MCFAs (**F**), LCFAs (**G**), and VLCFAs (**H**) in the samples in **A** (n = 5 mice/group). (**I**) Schema showing the desaturating and elongating reactions of the PUFAs with the reduction or accumulation of specific fatty acid molecules (from lipidomic data shown in **A**) and the downregulated corresponding enzymes (from RNA-seq data shown in Figure 3D) in *Qk*-iCKO mice relative to controls. The reduction in fatty acid desaturases is shown in light blue, and the reduction in enzymes of the fatty acid elongation cycle is shown in dark blue. The scale factor indicates a log2-fold change in the fatty acid concentration between *Qk*-iCKO mice and controls. (**J**) Quantification of the product/substrate ratios of representative fatty acid-elongating reactions in the samples in **A** (n = 5 mice/group). (**K**) Representative images showing the severe abnormal hind limb weakness (second panel from the left, red arrow) and paresis (sixth panel from the left, red arrow) of *Qk*-iCKO mice fed an ND or HFD for 5 weeks after tamoxifen injection. (**L**) Representative images of staining of FluoroMyelin in the caudoputamen tissues of the experimental mice in **K**. Images were taken from the regions of the red-boxed areas in the schema (left panel). Scale bars, 50 μm. Data are mean ± s.d.; student's t test. *$P < 0.05$; **$P < 0.01$; ***$P < 0.001$; ****$P < 0.0001$; ns, not significant.

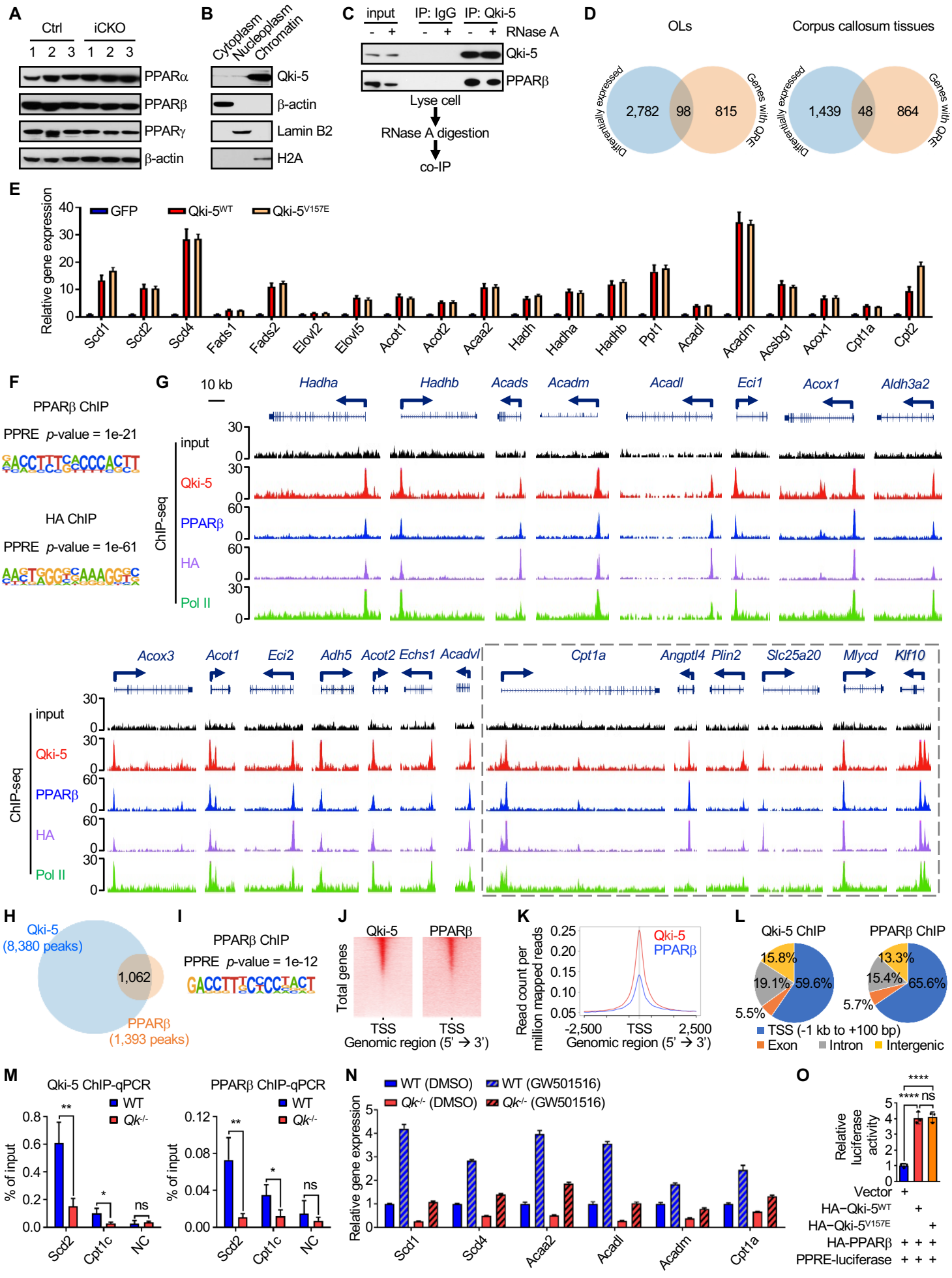
A
Ctrl
iCKO
1 2 3 1 2 3
PPARα
PPARβ
PPARγ
β-actin
B
Cytoplasm
Nucleoplasm
Chromatin
Qki-5
β-actin
Lamin B2
H2A
C
input
IP: IgG
IP: Qki-5
RNase A
Qki-5
PPARβ
Lyse cell
RNase A digestion
co-IP
D
OLs
Corpus callosum tissues
Differentially expressed
Genes with QRE
2,782
98
815
1,439
48
864
E
Relative gene expression
GFP
Qki-5WT
Qki-5V157E
Scd1
Scd2
Scd4
Fads1
Fads2
Elovl2
Elovl5
Acot1
Acot2
Acaa2
Hadh
Hadha
Hadhb
Ppt1
Acadl
Acadm
Acsbg1
Acox1
Cpt1a
Cpt2
F
PPARβ ChIP
PPRE p-value = 1e-21
HA ChIP
PPRE p-value = 1e-61
G
10 kb
Hadha
Hadhb
Acads
Acadm
Acadl
Eci1
Acox1
Aldh3a2
ChIP-seq
input
Qki-5
PPARβ
HA
Pol II
Acox3
Acot1
Eci2
Adh5
Acot2
Echs1
Acadvl
Cpt1a
Angptl4
Plin2
Slc25a20
Mlycd
Klf10
H
Qki-5
(8,380 peaks)
1,062
PPARβ
(1,393 peaks)
I
PPARβ ChIP
PPRE p-value = 1e-12
J
Qki-5
PPARβ
Total genes
TSS
TSS
Genomic region (5' → 3')
K
Read count per million mapped reads
Qki-5
PPARβ
-2,500
TSS
2,500
Genomic region (5' → 3')
L
Qki-5 ChIP
PPARβ ChIP
15.8%
19.1%
59.6%
5.5%
13.3%
15.4%
65.6%
5.7%
TSS (-1 kb to +100 bp)
Exon
Intron
Intergenic
M
Qki-5 ChIP-qPCR
PPARβ ChIP-qPCR
WT
Qk-/-
% of input
Scd2
Cpt1c
NC
N
WT (DMSO)
WT (GW501516)
Qk-/- (DMSO)
Qk-/- (GW501516)
Relative gene expression
Scd1
Scd4
Acaa2
Acadl
Acadm
Cpt1a
O
Relative luciferase activity
****
ns
Vector
HA−Qki-5WT
HA−Qki-5V157E
HA-PPARβ
PPRE-luciferase

Supplemental Figure 6. Qki-5 interacts with PPARβ to regulate the transcription of genes involved in fatty acid metabolism. (**A**) Immunoblots showing the expression of all homologs of PPAR in the corpus callosum tissues of *Qk*-iCKO mice and controls 5 weeks after tamoxifen injection. (**B**) Immunoblots showing the expression of Qki-5 in the subcellular fractions of differentiated oligodendrocytes. (**C**) Co-IP of Qki-5 and PPARβ in differentiated oligodendrocytes in which the cell lysate was treated with RNase A. (**D**) Venn diagram depicting the overlap between the differentially expressed genes (*Qk*-iCKO group versus the control group) and genes with QRE in freshly isolated mouse oligodendrocytes (left) and adult corpus callosum tissues (right). (**E**) RT-qPCR evaluation of the expression levels of genes involved in fatty acid metabolism in $Qk^{-/-}$ cells with ectopically expressed Qki-5^{WT}, Qki-5^{V157E}, or GFP. (**F**) Significant enrichment of PPRE motifs in PPARβ- and HA-binding events from differentiated oligodendrocytes with ectopic expression of HA-PPARβ. (**G**) Representative ChIP-seq binding peaks of Qki-5, PPARβ, HA, and Pol II on gene loci associated with fatty acid metabolism. The ChIP-seq peaks on six known PPARβ target genes are indicated in dotted box. (**H**) Overlap of ChIP-seq peak sets of Qki-5 and PPARβ in freshly isolated mouse oligodendrocytes. (**I**) Significant enrichment of PPRE motif in PPARβ-binding events from freshly isolated mouse oligodendrocytes. (**J**) ChIP-seq density heat maps of Qki-5 and PPARβ within ± 1 kb of the TSS in freshly isolated mouse oligodendrocytes. All peaks are rank ordered from high to low Qki-5 occupancy. (**K**) Average genome-wide occupancies of Qki-5 and PPARβ within ± 2.5 kb of the TSS in freshly isolated mouse oligodendrocytes. (**L**) Genomic global distribution of the ChIP-seq peaks of Qki-5 and PPARβ in freshly isolated mouse oligodendrocytes. (**M**) ChIP-qPCR showing the recruitment of Qki-5 and PPARβ to chromatin in WT and $Qk^{-/-}$ differentiated oligodendrocytes. NC, negative control. (**N**) RT-qPCR showing the transcriptional levels of representative genes involved in fatty acid metabolism in WT and $Qk^{-/-}$ differentiated oligodendrocytes treated with 100 nM GW501516 or vehicle (DMSO) for 48 hours. (**O**) Bar graph showing the expression of PPAR-responsive luciferase reporter in HEK293T cells with ectopically expressed Qki-5 (WT or V157E mutant) or empty vector. Data are representative of 3 independent experiments (**A**-**C**, **E**, and **M**-**O**). Data are mean ± s.d.; student's *t* test (**M**); one-way ANOVA followed by Bonferroni's post hoc test (**O**). *$P < 0.05$; **$P < 0.01$; ****$P < 0.0001$; ns, not significant.

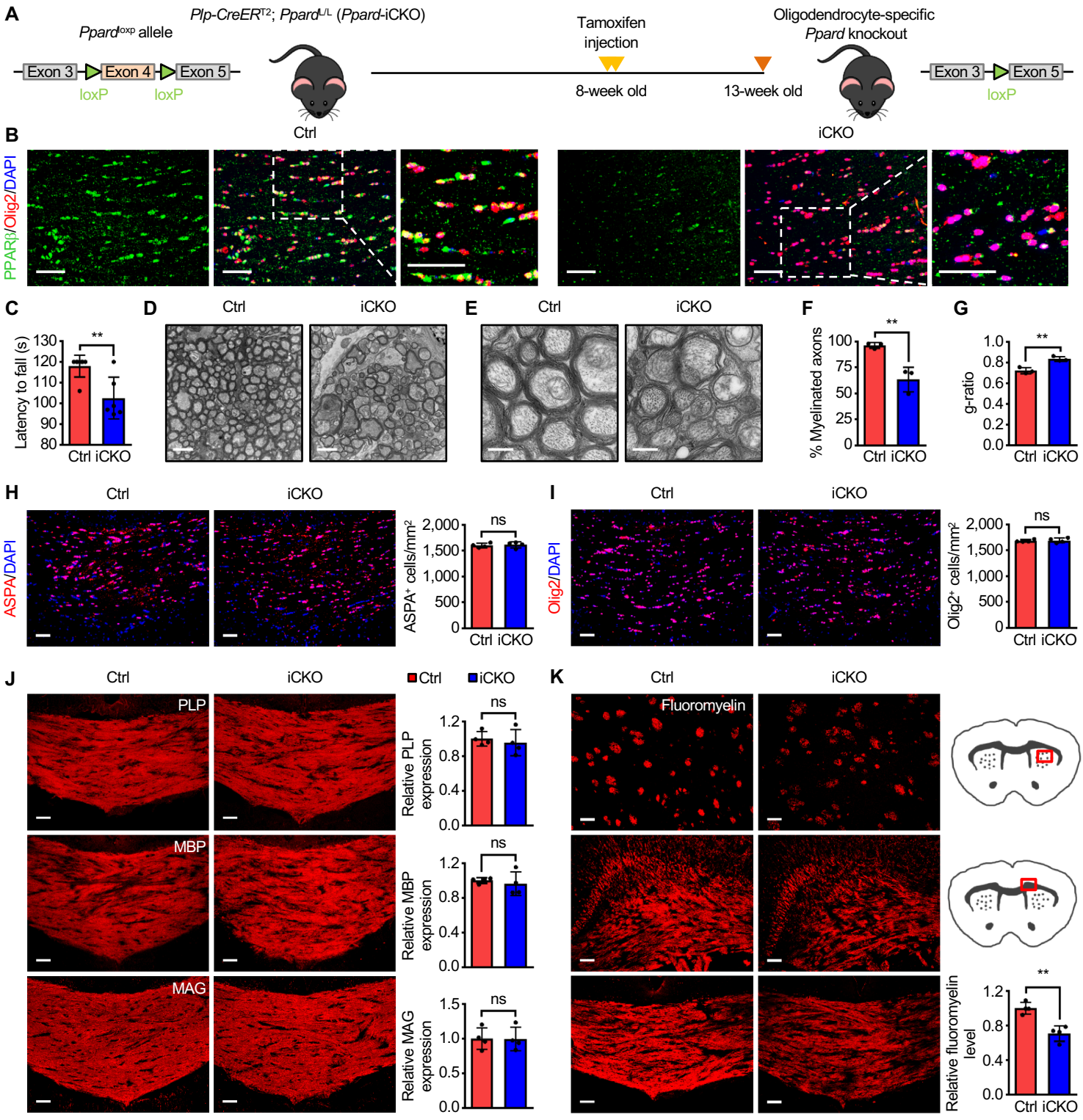

Supplemental Figure 7. Ablation of *Ppard* in mature myelinating oligodendrocytes leads to demyelination with reduction in myelin lipids. (**A**) Schema showing the *Ppard*^{Loxp} allele and the generation of oligodendrocyte-specific *Ppard*-knockout mice. (**B**) Representative images of immunofluorescent staining of PPARβ-Olig2 in the corpus callosum tissues of *Ppard*-iCKO mice and controls 5 weeks after tamoxifen injection. $n = 4$ mice/group. Scale bars, 50 μm. (**C**) Latency to fall (s) off the rotarod (20 r.p.m.) for *Ppard*-iCKO mice and controls 5 weeks after tamoxifen injection ($n = 7$ mice in the control group, $n = 6$ mice in the *Ppard*-iCKO group). (**D-G**) Representative electron micrographs and quantification of the optic nerves of *Ppard*-iCKO mice and control mice 5 weeks after tamoxifen injection ($n = 3$ mice/group). Scale bars, 2 μm (**D**); 500 nm (**E**). (**H** and **I**), Representative images and quantification of immunofluorescent staining of ASPA and Olig2 in the corpus callosum tissues of the experimental mice in **B** ($n = 4$ mice/group). Scale bars, 50 μm. (**J**) Representative images and quantification of immunofluorescent staining of PLP, MBP, and MAG in the corpus callosum tissues of the experimental mice in **B** ($n = 4$ mice/group). Scale bars, 50 μm. (**K**) Representative images and quantification of staining of FluoroMyelin in the experimental mice in **B** ($n = 4$ mice/group). Images were taken from the regions of the red-boxed areas in the schema. Scale bars, 50 μm. Data are mean ± s.d.; student's *t* test. $^{**}P < 0.01$; ns, not significant.

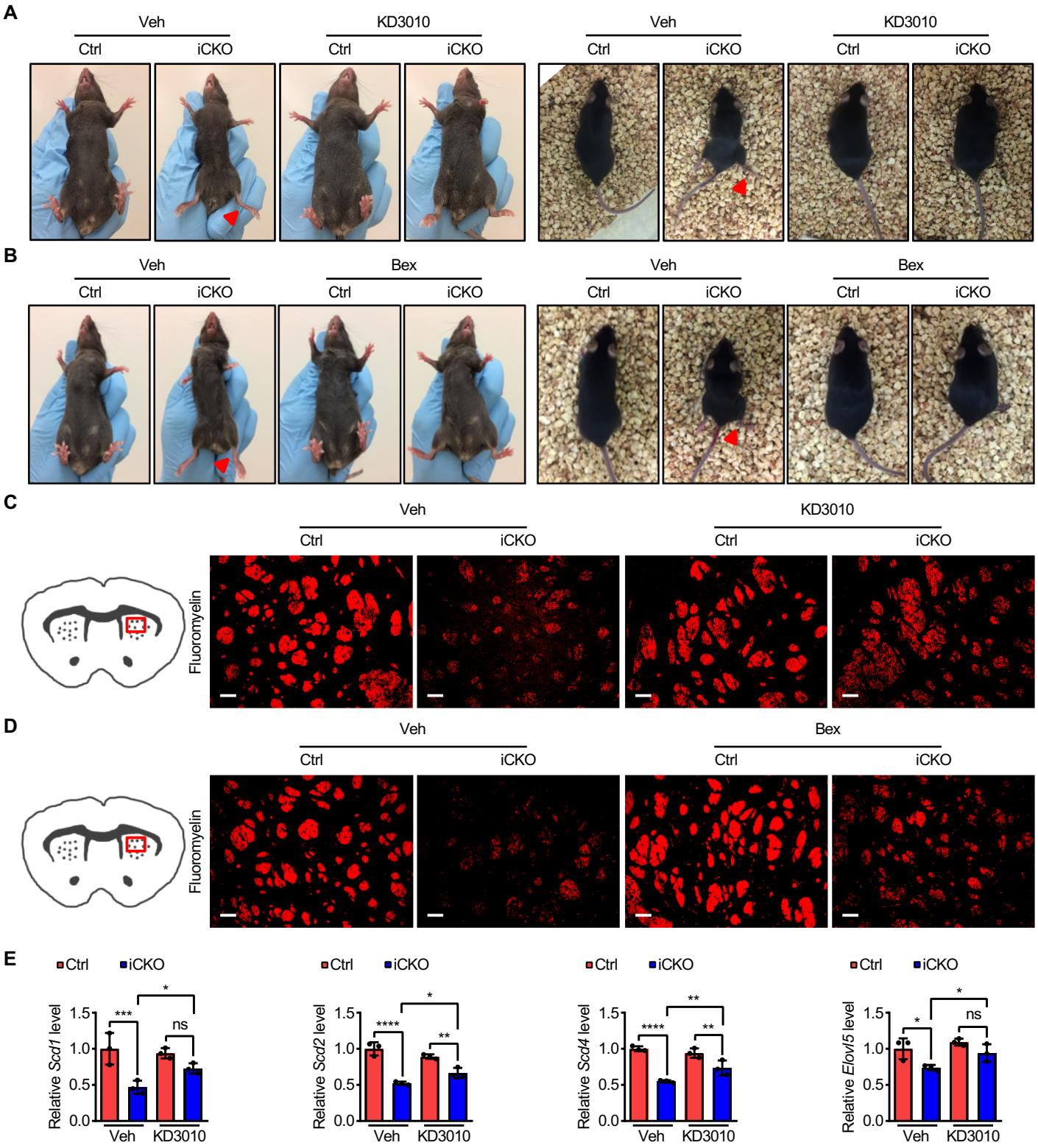

Supplemental Figure 8. PPARβ and RXR agonists alleviate Qki depletion-induced demyelination. (**A** and **B**) Representative images showing severe abnormal hind limb weakness (second panel from the left, red arrow) and paresis (sixth panel from the left, red arrow) in *Qk*-iCKO mice receiving daily oral administration of KD3010, Bex, or Veh for 5 weeks after tamoxifen injection. (**C** and **D**) Representative images of staining of FluoroMyelin in the caudoputamen tissues of *Qk*-iCKO mice and controls receiving daily oral administration of KD3010, Bex, or Veh for 5 weeks after tamoxifen injection. Images were obtained from the regions of the red-boxed areas in the schema (left panel). Scale bars, 50 μm. (**E**) Quantification of the expression level of genes involved in fatty acid metabolism in the corpus callosum tissues of *Qk*-iCKO mice and controls receiving KD3010 or Veh for 5 weeks after tamoxifen injection by RT-qPCR. Data are mean ± s.d.; one-way ANOVA with Fisher's LSD test. **P* < 0.05; ***P* < 0.01; ****P* < 0.001; *****P* < 0.0001; ns, not significant.

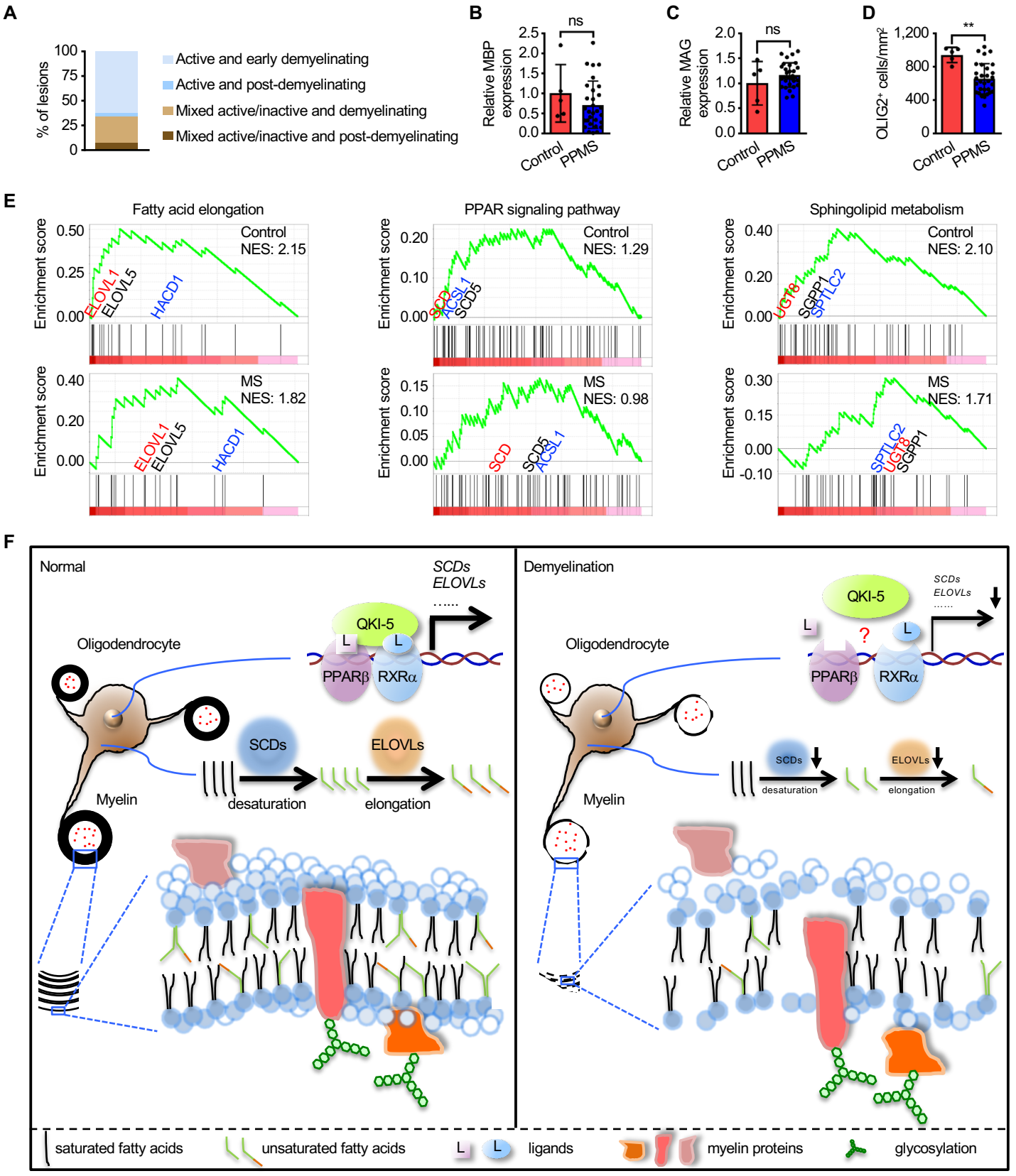

Supplemental Figure 9. Myelin lipid metabolism is preferentially reduced in MS lesions. (**A**) Percentage of MS lesions with different inflammatory and demyelinating activities. (**B-D**) Quantification of immunofluorescent staining of MBP (**B**), MAG (**C**), and OLIG2 (**D**) in the frontal lobes of 5 neurological disease-free human brains (control) and 30 lesions from 6 patients with PPMS. (**E**) Comparison of the GSEA signatures of lipid metabolism pathways between the MS lesions and the controls. (**F**) Schematic of the essential role of Qki-PPARβ-RXRα complex-regulated fatty acid desaturation and elongation in mature myelin maintenance. Data are mean ± s.d.; student's *t* test. $^{**}P < 0.01$; ns, not significant.

Supplemental Video 1. Severe abnormal hind limb weakness and paresis in *Qk*-iCKO mice. 8-week-old *Qk*-iCKO mice and control mice were injected with tamoxifen and the severity of abnormal hind limb weakness and paresis of these animals was recorded 5 weeks after injection.

Supplemental Video 2. High-fat diet alleviates Qki-depletion–induced neurological deficits. 8-week-old tamoxifen-injected *Qk*-iCKO mice and control mice were fed either a normal diet (ND) or the high-fat diet (HFD). The severity of abnormal hind limb weakness and paresis of these animals was recorded 5 weeks after treatment.

Supplemental Video 3. PPARβ agonist alleviates Qki-depletion–induced neurological deficits. 8-week-old tamoxifen-injected *Qk*-iCKO mice and control mice were orally administered 50 mg/kg/day KD3010 or vehicle (Veh). The severity of abnormal hind limb weakness and paresis of these animals was recorded 5 weeks after treatment.

Supplemental Video 4. RXR agonist alleviates Qki-depletion–induced neurological deficits. 8-week-old tamoxifen-injected *Qk*-iCKO mice and control mice were orally administered 100 mg/kg/day bexarotene (Bex) or vehicle. The severity of abnormal hind limb weakness and paresis of these animals was recorded 5 weeks after treatment.

Supplemental Table 1 (separate Excel file). Lipidomic analysis of the concentrations of lipids in the spinal cords of *Qk*-iCKO mice and control mice. Tamoxifen was administered to 8-week-old *Qk*-iCKO mice and control mice (5 in each group), and their spinal cords were collected 5 weeks later for further lipidomic analysis.

Supplemental Table 2 (separate Excel file). Lipidomic analysis of the compositions of lipids in the spinal cords of *Qk*-iCKO mice and control mice. Tamoxifen was administered to 8-week-old *Qk*-iCKO mice and control mice (5 in each group), and their spinal cords were collected 5 weeks later for further lipidomic analysis.

Supplemental Table 3. Human brain sample information.

RMMSC[A] #	Tissue type	Age at death	PMI[B]	Sex	Cause of death	Disease duration	Disease-modifying therapies / immunomodulat-ory therapy
408	Control	74	48 hours	M	unknown	N/A	N/A
482	Control	46	N/A	F	unknown	N/A	N/A
487	Control	59	19 hours	M	unknown	N/A	N/A
489	Control	73	N/A	F	unknown	N/A	N/A
503	Control	55	N/A	F	unknown	N/A	N/A
436	Primary progressive multiple sclerosis	60	10 hours	M	unknown	unknown	unknown
438	Primary progressive multiple sclerosis	75	20 hours	F	unknown	36 years	none
449	Primary slow progressive multiple sclerosis	74	7 hours	F	unknown	unknown	none
495	Primary slow progressive multiple sclerosis	78	20 hours	F	Respiratory failure	33 years	none
507	Primary progressive multiple sclerosis	69	0 hour	F	unknown	46 years	Natalizumab
534	Primary slow progressive multiple sclerosis	71	43 hours	F	unknown	symptoms 43 years; diagnosed 23 years	unknown

[A]Rocky Mountain Multiple Sclerosis Center

[B]postmortem interval

Supplemental Table 3. Human brain sample information. The patients' age at the time of death, sex, postmortem interval, pathological diagnosis, cause of death, disease duration, and disease-modifying therapies are shown.

Supplemental Table 4. Primer sequences.

Primer Name	Primer sequence	Comments
Scd1-Forward	CCTCTTCGGGATTTTCTACTACAT	RT-qPCR
Scd1-Reverse	TCCAGTTTTCCGCCCTTCTC	RT-qPCR
Scd2-Forward	AAGATGATCTATATGACCCCACCT	RT-qPCR
Scd2-Reverse	CACGTCATTCTGGAACGCCA	RT-qPCR
Scd4-Forward	TGTCTGACCTGAAAGCCGAG	RT-qPCR
Scd4-Reverse	GTGGAAGCCCTCGCCTAAAG	RT-qPCR
Fads1-Forward	GTGATCGACCGGAAGGTGTA	RT-qPCR
Fads1-Reverse	AGCGCTTTATTCTTGGTGGGT	RT-qPCR
Fads2-Forward	CATCGACCGCAAGGTCTACA	RT-qPCR
Fads2-Reverse	TCTGAGAGCTTTTGCCACGG	RT-qPCR
Elovl2-Forward	TACCCTGGACAGCGCATCG	RT-qPCR
Elovl2-Reverse	AGAGGATGAGCTCCACCAGCA	RT-qPCR
Elovl5-Forward	ATGGAACATTTCGATGCGTCA	RT-qPCR
Elovl5-Reverse	GTCCCAGCCATACAATGAGTAAG	RT-qPCR
Acot1-Forward	ATACCCCCTGTGACTATCCTGA	RT-qPCR
Acot1-Reverse	CAAACACTCACTACCCAACTGT	RT-qPCR
Acot2-Forward	CTCTTCCTGCCCCCAGAACC	RT-qPCR
Acot2-Reverse	CAGCCCAATTCCAGGTCCTT	RT-qPCR
Acaa2-Forward	CTGCTACGAGGTGTGTTCATC	RT-qPCR
Acaa2-Reverse	AGCTCTGCATGACATTGCCC	RT-qPCR
Hadh-Forward	TCGTGAACCGACTCTTGGTG	RT-qPCR
Hadh-Reverse	ATTTCATGCCACCCGTCCAA	RT-qPCR
Hadha-Forward	TGCATTTGCCGCAGCTTTAC	RT-qPCR
Hadha-Reverse	GTTGGCCCAGATTTCGTTCA	RT-qPCR
Hadhb-Forward	ACTACATCAAAATGGGCTCTCAG	RT-qPCR
Hadhb-Reverse	AGCAGAAATGGAATGCGGACC	RT-qPCR
Ppt1-Forward	ACCGCTGGTGATCTGGCAT	RT-qPCR
Ppt1-Reverse	TCTCCACATCCTCCATCATGTTCT	RT-qPCR
Acadl-Forward	TCTTTTCCTCGGAGCATGACA	RT-qPCR
Acadl-Reverse	GACCTCTCTACTCACTTCTCCAG	RT-qPCR
Acadm-Forward	AGGGTTTAGTTTTGAGTTGACGG	RT-qPCR
Acadm-Reverse	CCCCGCTTTTGTCATATTCCG	RT-qPCR
Acsbg1-Forward	ATGCCACGCGGTTCTGAAG	RT-qPCR
Acsbg1-Reverse	GAGCTGGTTTGCGAGTTGTCT	RT-qPCR
Acox1-Forward	TAACTTCCTCACTCGAAGCCA	RT-qPCR
Acox1-Reverse	AGTTCCATGACCCATCTCTGTC	RT-qPCR
Cpt1a-Forward	CTCCGCCTGAGCCATGAAG	RT-qPCR
Cpt1a-Reverse	CACCAGTGATGATGCCATTCT	RT-qPCR
Cpt2-Forward	CAGCACAGCATCGTACCCA	RT-qPCR
Cpt2-Reverse	TCCCAATGCCGTTCTCAAAAT	RT-qPCR
Actb-Forward	CCACCATGTACCCAGGCATT	RT-qPCR
Actb-Reverse	CCGATCCACACAGAGTACTT	RT-qPCR

Continued		
mC-*Scd2*-Pmt-Forward	ATGGAGTTGCAAGTGGTCGG	ChIP-qPCR
mC-*Scd2*-Pmt-Reverse	GCTTCAGCGCTTTCTCTGGA	ChIP-qPCR
mC-*Cpt1c*-Pmt-Forward	CATCGAGGGATGCTGGTGAG	ChIP-qPCR
mC-*Cpt1c*-Pmt-Reverse	GCGAGTAGGGCTTCTCCATC	ChIP-qPCR
mC-NC-Forward	ATGCCTAACTTCCAGTTCCAGG	ChIP-qPCR
mC-NC-Reverse	AGCTTAGAGCAGAAAGCTGGT	ChIP-qPCR

Supplemental Table 4. Primer sequences. A complete list of the sequences of the primers used in this study is shown.

Supplemental Methods

RNA isolation and real-time qPCR. RNA was extracted from the corpus callosum tissues of the mouse brains, freshly isolated mouse oligodendrocytes, NSCs, and differentiated oligodendrocytes using an RNeasy Mini Kit, according to the manufacturer's instructions (Qiagen). Two micrograms of RNA were reverse transcribed to cDNA using SuperScript III First-Strand Synthesis SuperMix (Thermo Fisher Scientific), and real-time qPCR was performed using iTaq Universal SYBR Green Supermix (Bio-rad) in an Applied Biosystems 7500 Fast Real-Time PCR system. The relative transcription levels of the genes of interest were normalized against *Actb* and calculated using the ΔΔCT method. A complete list of the primer sequences used in this study can be found in Supplemental Table 4.

GSEA in human tissue samples. Raw gene expression profiling files were downloaded from the Gene Expression Omnibus under accession number GSE38010 (40). The latest version of custom CDF files (v22) (59, 60) was used to map probes from the Affymetrix Human Genome U133 Plus 2.0 Array to the Ensemble transcript database, resulting in robust multi-array average-normalized and log-transformed gene expression values (61). A single-sample GSEA was performed on the expression profiles of 4 cases (CAP1, CAP2, CP1, and CP2) and 2 controls (control 1 and control 2) for 8 pathways (fatty acid metabolism [KEGG: 01212], fatty acid biosynthesis [KEGG: 00061], biosynthesis of unsaturated fatty acids [KEGG: 01040], fatty acid elongation [KEGG: 00062], fatty acid degradation [KEGG: 00071], PPAR signaling pathway [KEGG: 03320], sphingolipid metabolism [KEGG: 00600], and glycerophospholipid metabolism [KEGG: 00564]). Normalized enrichment scores were calculated for representation and further

analyses. GSEA (v2.2.4) was used to generate the representative enrichment plots for pathways per sample (58).

Genome-wide computational analysis for RNA motifs of Qki. A computational screening of the mouse reference genome (mm10 version) with the QRE motif (UACUAAC) was performed on MotifMap (http://motifmap.ics.uci.edu) (62).

Immunoprecipitation and immunoblotting. Differentiated oligodendrocytes were crosslinked by 1% formaldehyde for 10 minutes and lysed in NP-40 buffer (50 mM Tris-HCl [pH 7.5], 150 mM NaCl, 5 mM EDTA, and 0.3% NP-40) for 30 minutes at 4°C. The whole-cell lysate was sheared using a Bioruptor Pico sonication device (Diagenode) for 30 cycles (30 seconds on, 30 seconds off) and centrifuged at 13,000 g at 4°C for 15 minutes. The supernatant was incubated with antibodies against Qki-5 (immunizing rabbit with a short synthetic peptide [CGAVATKVRRHDMRVHPYQRIVTADRAATGN]), HA (ab18181; Abcam), PPARβ (PA1-823A; Thermo Fisher Scientific), or normal immunoglobulin G overnight at 4°C. Magnetic beads with recombinant protein G (Thermo Fisher Scientific) were added to the immunoprecipitation system for another 2 hours at 4°C. The immunoprecipitates were washed extensively with NP-40 buffer 3 times, and the bound proteins were boiled with SDS-PAGE sample buffer at 95°C for 20 minutes before further immunoblotting.

Brain tissues were homogenized in NP-40 buffer and lysed in the same manner as described above. Protein concentrations were measured using a DC protein assay (Bio-rad). We then subjected 20 to 40 μg of protein to a standard immunoblotting protocol. The following antibodies were used according to their manufacturer's directions: anti-PLP (ab105784), anti-

PPARα (ab24509), and anti-HA (ab18181) were from Abcam; anti-PPARγ (#2435), anti-RXRα (#3085), and anti-Lamin B2 (#13823) were from Cell Signaling Technology; anti-MOG (sc-73330) and anti-histone H2A (sc-10807) were from Santa Cruz Biotechnology; anti-PPARβ (PA1-823A) was from Thermo Fisher Scientific; anti-RXRβ (NBP1-30897) was from Novus Biologicals; RXRγ (CPA2042) was from Cohesion Biosciences; anti-MBP (SMI-94R) was from Covance; anti–Qki-5 (IHC-00574) was from Bethyl Laboratories; and anti–β-actin (A5441) was from Sigma-Aldrich.

RNase A treatment. The differentiated oligodendrocytes were washed once with PBS, washed again with ASE buffer (20 mM Tris-HCl [pH 7.5], 0.5 mM EGTA, and 5 mM $MgCl_2$), and permeabilized with ASE buffer containing 0.1% Triton X-100 at room temperature for 5 minutes. The cells were treated with 100 μg/mL RNase A (DNase- and protease-free; Thermo Fisher Scientific) at room temperature for 20 minutes to digest RNA in the living cells (63). Cells were washed with PBS and subjected to crosslinking, sonication, and co-IP experiments, as described above. Alternatively, the differentiated oligodendrocytes were lysed in NP-40 buffer at 4°C for 30 minutes, followed by digestion with 100 μg/mL RNase A at room temperature for 20 minutes. The cell lysates were then used for co-IP.

ChIP-seq and ChIP-qPCR. ChIP assays were carried out as described previously (64). The sheared chromatin from differentiated oligodendrocytes with ectopic expression of HA-PPARβ (with lentiviral plasmid pInducer20) or freshly isolated mouse oligodendrocytes was incubated with anti–Qki-5 (immunizing rabbit with a short synthetic peptide [CGAVATKVRRHDMRVHPYQRIVTADRAATGN]), anti-PPARβ (PA1-823A; Thermo Fisher

Scientific), anti-HA (#3724S; Cell Signaling Technology), or anti-Pol II (ab817; Abcam) antibodies in High Salt Buffer (50 mM HEPES-NaOH [pH 7.5], 300 mM NaCl, 1 mM EDTA, 1% Triton, 0.1% SDS, and 0.1% sodium deoxycholate with freshly added protease inhibitor) overnight at 4°C. The protein-DNA complexes were immobilized on prewashed protein A/G agarose beads (Smart-lifesciences). After several washes, the bound fractions were eluted and reverse crosslinked in the elution buffer (50 mM Tris-HCl [pH 8.0], 10 mM EDTA, and 1% SDS) and digested with RNase A and proteinase K at 65°C for 4 hours, DNA samples were then purified using a PCR purification kit (Qiagen). Libraries were generated by VAHTS Universal DNA Library Prep Kit (Vazyme) and sequenced by Illumina HiSeq X Ten or NovaSeq 6000 (Jiangxi Haplox Clinical Lab Cen, Ltd). The FASTQ data were trimmed by trim_galore (v0.4.4_dev) and mapped to the mouse genome (mm10 version) using bowtie (v1.2.2) (65), then peaks were identified by homer (v4.10.1) (66) with the following steps: makeTagDirectory and findPeaks Sample_tag -style factor -size auto -minDist default -i Input_tag -fdr 0.001. The top 1,000 peaks of PPARβ and HA from differentiated oligodendrocytes and the top 300 peaks of PPARβ from freshly isolated mouse oligodendrocytes were used for motif search. Motif was called by homer with findMotifsGenome.pl -size 300 -len 14,15,16 -mis 3. Signal plots and Heatmaps were generated with ngsplot (67). ChIP-qPCR was performed using iTaq Universal SYBR Green Supermix, as described above. A complete list of the sequences of the primers used in this study can be found in Supplemental Table 4.

References

59. Dai M, et al. Evolving gene/transcript definitions significantly alter the interpretation of GeneChip data. *Nucleic Acids Res.* 2005;33(20):e175.

60. Sandberg R, Larsson O. Improved precision and accuracy for microarrays using updated probe set definitions. *BMC bioinformatics.* 2007;8(1):48.

61. Bengtsson H, Ray A, Spellman P, Speed TP. A single-sample method for normalizing and combining full-resolution copy numbers from multiple platforms, labs and analysis methods. *Bioinformatics.* 2009;25(7):861-867.

62. Liu Y, Sun S, Bredy T, Wood M, Spitale RC, Baldi P. MotifMap-RNA: a genome-wide map of RBP binding sites. *Bioinformatics.* 2017;33(13):2029-2031.

63. Chamousset D, et al. RRP1B targets PP1 to mammalian cell nucleoli and is associated with Pre-60S ribosomal subunits. *Mol Biol Cell.* 2010;21(23):4212-4226.

64. Lan F, et al. A histone H3 lysine 27 demethylase regulates animal posterior development. *Nature.* 2007;449(7163):689-694.

65. Langmead B, Trapnell C, Pop M, Salzberg SL. Ultrafast and memory-efficient alignment of short DNA sequences to the human genome. *Genome Biol.* 2009;10(3):R25.

66. Heinz S, et al. Simple combinations of lineage-determining transcription factors prime cis-regulatory elements required for macrophage and B cell identities. *Mol Cell.* 2010;38(4):576-589.

67. Shen L, Shao N, Liu X, Nestler E. ngs.plot: Quick mining and visualization of next-generation sequencing data by integrating genomic databases. *BMC Genomics.* 2014;15:284.